Interatomic Spin Coupling in Manganese Clusters Registered on Graphene

Jindong Ren, Haiming Guo, Jinbo Pan, Yan-Fang Zhang, Yifeng Yang, Xu Wu, Shixuan Du, Min Ouyang, and Hong-Jun Gao

Phys. Rev. Lett. **119**, 176806 — Published 27 October 2017

DOI: 10.1103/PhysRevLett.119.176806

(Submitted to Phys. Rev. Lett.)

Inter-atomic Spin Coupling in Manganese Clusters Registered on Graphene

Jindong Ren[1,†], Haiming Guo[1,†,*], Jinbo Pan[1,†], Yan-Fang Zhang[1], Yi-feng Yang[1], Xu Wu[1], Shixuan Du[1], Min Ouyang[2] and Hong-Jun Gao[1]

[1]Institute of Physics & University of Chinese Academy of Sciences, Chinese Academy of Sciences, Beijing 100190, China

[2]Department of Physics, University of Maryland, College Park, MD 20742-4111, USA

Abstract: We have investigated different inter-atomic spin interactions in graphene regulated Mn atomic clusters by low-temperature scanning tunneling microscopy and magnetic field dependent inelastic spin excitation spectroscopy. All dimers observed exhibit an antiferromagnetic (AFM) singlet ground state and spin transition from the singlet to triplet states, but their AFM coupling strength shows unique dependence on their site registration on the graphene template, which agrees well with density function theory (DFT) calculations. Even more importantly, intriguing spin coupling can be found in the graphene mediated Mn trimers, which manifest multi-level spin excitations. In combination with Heisenberg spin modeling and first-principles numerical simulation, exclusive non-collinear spin configuration of Mn trimer regulated by the graphene template can be determined, and our observed experimental exchange energies cannot be understood by direct spin exchange mechanism, but suggesting non-local Ruderman-Kittel-Kasuya-Yosida (RKKY) indirect spin exchange mechanism through substrate modulation, which has not yet been achieved in graphene so far. Our results of both dimers and trimers unanimously suggest that the graphene/Ru substrate acts as not only a unique molecular template but also a host lattice to mediate local and non-local spin interactions in Mn clusters.

PACS numbers: 74.55.+v, 75.10.Jm, 75.30.Hx,75.75.Lf

†These authors contributed equally to this work.

*Correspondence and requests for materials should be addressed to H. M. Guo (e-mail: hmguo@iphy.ac.cn)

Magnetic nanoclusters represent an ideal toolbox to understand atomic scale spin interactions and size evolution of magnetic properties, as well as to construct functional spin based nanodevices as building blocks [1, 2]. Such magnetic nanostructures are typically fabricated by either epitaxial or lithographic techniques on limited choice of substrates [3, 4], or by atomic manipulation with various scanning probe approaches [5, 6]. Nevertheless, they are all either hard to control at the very small scale or slow process requiring demanding fabrication time. Recently, graphene has exhibited many attractive physical properties desirable for spintronics, including for example small spin-orbit coupling and long spin diffusion length [7-14]. Moreover, periodically rippled graphene modulated by its underneath substrate has been demonstrated to act as a unique atomic scale template for molecular self-assembly to tailor molecule-molecule interactions or molecule-substrate interactions [15-19].

Study of direct assembly of magnetic atoms on graphene surface, however, has been lacking, but it represents an emerging class of magnetic nanostructures that can potentially possess template modulated interatomic magnetic interactions uniformly at the nanoscale [20-25]. Additional importantly, intimate contact between graphene and metal substrate can modify electronic properties of graphene through, for example, local distortion of atomic orbitals of carbon atoms arising from periodical structural fine-tailoring in a moiré superlattice [26] as well as conduction carrier doping via electron transfer mechanism [27-30]. This can therefore provide a new avenue to mediate and tailor spin exchange interactions among magnetic atoms in a cluster, resulting in new magnetic properties uniquely defined by graphene template that will be otherwise challenging in current existing techniques. For example, doped conduction carriers in graphene can potentially act as a host to mediate non-local spin interactions through Ruderman-Kittel-Kasuya-Yosida (RKKY) indirect exchange process, which has been ubiquitously studied on a variety of metal substrates but related work on graphene has been lacking [31-33].

In this letter, we have investigated various atomic scale spin interactions within Mn dimers and trimers that are regulated by the underneath epitaxial monolayer graphene on Ru(0001) surface. It has been demonstrated that lattice mismatch between graphene and Ru(0001) surface can induce a periodical surface corrugation of graphene, forming a unique strained superlattice consisting of three structural regions in a unit cell: atop, fcc and hcp sites (Fig.1(a)). These three regions are defined based on their different atomic stacking modes, and have manifested distinct structural characteristics [19, 29, 30] (see Fig. S1(a)). By combining scanning probe imaging with magnetic field dependent

inelastic spin excitation spectra (ISES), this can allow us to correlate as-measured local spin spectroscopy with different sized Mn nanoclusters registered at different locations of the rippled graphene (Fig. 1(a)). For example, antiferromagnetic Mn dimers are found to stay preferentially on the atop-edge and fcc sites of the graphene/Ru substrate, but with a dramatic difference in the AFM coupling strength. Importantly, more intriguing spin interactions in Mn trimers have also been observed. With the assistance of theoretical modeling spin configuration of trimers registered on the graphene substrate can be determined, which unravels a long-range RKKY indirect spin exchange interaction.

To achieve small Mn clusters on graphene/Ru(0001) surface, we have first employed a previously developed technique (Supplementary S1) to epitaxially grow monolayer graphene on Ru substrate [29, 30] and then deposit Mn atoms in situ at ~20 K [19, 34]. The possibility of unintentionally doped H atoms onto the Mn clusters can be safely excluded in our experiments [11, 35] (see Supplementary S3). Under our current deposition conditions, the majority of Mn atomic clusters are found as dimers, but occasionally trimers are also identified [36-38]. Notably, we have observed a strong correlation between occupation sites of Mn dimers and moiré pattern: the Mn dimer adsorption is clearly site-specific on the graphene/Ru(0001) surface, with statistical results summarized in Fig. 1(b). The Mn dimers occupy prevailingly (~80%) the edge position of atop regions of graphene, and the rest stay at the fcc regions (~ 20%) (see Fig. 1(a) and S2). No dimer is found at the hcp sites. This observation of preferential adsorption can be attributed to the difference in binding energies of these sites (see Table 1).

The *dI/dV-V* spectra of Mn dimers located at the atop-edge and fcc sites (Fig. 1(c)) show similar symmetric stepwise feature with respect to the Fermi level, suggesting a spin-change transition of Mn dimers from the AFM to ferromagnetic (FM) states (Fig. 2(a)). This can be confirmed unambiguously by a more thorough study of magnetic field dependence to reveal evolution of the spin excitation spectra. The results for the atop-edge site are presented in Fig. 2(b), in which the single step at zero field splits into three distinct IETS excitation traits. Such splitting indicates spin-flipping transition from the AFM singlet state ($S = 0$) to the first excited state of a triplet ($S = 1$), which splits into $|1, 0\rangle$ and $|1, \pm1\rangle$ under the presence of magnetic field. Furthermore, corresponding g-factor can be determined to be $g = 1.86 \pm 0.02$ by linearly fitting the energy shift of step as $\Delta m g \mu_B B$ ($\Delta m = -1, 0, 1$), and the observed offset (about 0.2 meV) of the triplet straight lines at the zero field is produced by a

small magnetic anisotropy term [39] (see Fig. 2(c)). Figure 2(d) shows a schematic of spin configuration of a Mn dimer and their excitations under the magnetic field.

However, the zero-field onset energy of spin excitation shows dramatic difference at the different adsorption sites. The excitation step is located around 10 ± 2 mV for dimer at the edge of atop regions, as compared with 7 ± 2 mV for those on the fcc regions. This suggests that the AFM coupling strength J of the Mn dimers can be locally tuned by graphene template. Qualitatively, we believe the site-dependent AFM exchange energy is due to local spatial modulation of orbital bonding on the graphene/Ru. In the fcc and hcp regions, sp^2 hybridization in graphene can be corrupted due to strong coupling between the carbon and Ru atoms with enhanced sp^3 characteristics of carbon orbitals. This has been formerly predicted by comparing the computed projected density of states on p_z orbitals of carbon atom located in different regions of the graphene/Ru [26]. One direct effect of such spatially modulated local orbital hybridization is to form a stronger bonding with adsorbed Mn atom on top (that has a half-filled d shell) and to stabilize the FM state of a Mn dimer in the fcc and hcp regions with enlargement of adsorption energy (see Table 1). This effect can further result in smaller exchange energy of the Mn dimers accommodated in the fcc region, as compared with that of dimers located in the atop sites. We have evaluated these effects, and directly compared binding energies (E_{FM} or E_{AFM}) for both the FM and AFM states of a Mn dimer. For both the fcc and atop sites, the AFM coupling state is found to be the most energy favorable state. Furthermore, the coupling strengths J can be obtained from the difference between the binding energies in the FM and AFM states (E_{FM} - E_{AFM}), which are determined to be 8.2 and 7.4 meV for the atop-edge and fcc sites, respectively. These theoretical values agree with our experimental results (Table 1), and the rippled graphene can indeed offer unique opportunity to finely tailor nanoscale spin interactions as a role of template.

Table 1: Theoretical calculation results of the Mn dimer adsorbed at different sites of graphene/Ru(0001) surface.

	$d_{Mn\text{-}sub}$ (Å)	$d_{Mn\text{-}Mn}$ (Å)	E_{AFM} (eV)	E_{FM}-E_{AFM} (meV)	$J_{cal.}$ (meV)	$J_{exp.}$ (meV)
Mn@edge	5.06	2.60	-11.418	123	8.2	10 ± 2
Mn@fcc	4.35	2.66	-11.538	111	7.4	7 ± 2

E_{FM}, E_{AFM}: binding energies of Mn dimer for FM and AFM cases, respectively;
$J_{cal.}$, J_{exp}: coupling strengths derived from calculation and measured from experiment, respectively.

Such template effect can also allow formation of even more intriguing robust non-collinear spin systems with competing FM and AFM exchange interactions, which can be otherwise challenging by simple assembly of magnetic atoms on a plain substrate [6, 39]. Other than dimers, another stable spin configuration has been also occasionally observed in our study and can be assigned to be a spin trimer. As compared with dimers, trimers can possess much more complicated configurations under regulation of graphene template. For example, we have employed the DFT calculation [40-46] to evaluate possible stable configurations of trimer adsorbed at the atop-edge region. There exist four stable spin configurations for small Mn trimer (that is, we only consider the scenario that the inter-atomic distances within trimer are short enough to allow strong spin coupling), as show in Fig. 3. Interestingly, in addition to the linear chain configuration in which AFM coupling exists for two nearest neighboring atoms (Fig. 3(a)), as previously demonstrated for Mn chains on CuN substrates [6, 39], three non-collinear configurations can also become possible on the graphene/Ru substrate due to three-fold symmetry of hexagonal lattice of graphene substrate (Figs. 3(b) to 3(d)) [13, 14]. Such regulation through graphene template can therefore give rise to rich spin interactions, including AFM-AFM-FM and AFM-FM-FM, in an energetically favorable trimer configuration.

Figure 4(a) shows one Mn trimer observed on the graphene template. As compared with the ISES spectra of dimers, the Mn trimer has manifested much more complex spectral features. Three symmetric stepwise features appear near the Fermi level at 0.3 mV, 5.8 mV and 10.2 mV at the zero field, respectively (see Fig. 4(a)). Each of these three peaks manifests a distinct dependence on the magnetic field strength. With the increase of magnetic field strength, both the first and third steps shift to higher energy, while the second step shifts to lower energy, as shown in Fig. 4(a). The distinct field dependencies of these stepwise features are summarized in Fig. 4(b). Their corresponding g factor*s* can be determined as 2.17 ± 0.11, 2.03 ± 0.14 and 1.91 ± 0.17 for the first, second and third steps from such field dependent measurements, respectively.

These intriguing spectroscopic features can be understood by the Heisenberg spin model. The spin-assisted inelastic tunneling process should meet the spin excitation selection rules of $\Delta m = \pm 1$. At first, the linear chain configuration can be safely excluded from our scenario (see details in Supplementary S5). We have further evaluated the other three possible non-collinear triangular configurations of the Mn trimers. Figures 3(b)-3(d) suggest that the AFM interaction should exist in a stable triangular configuration. Theoretically, such non-collinear trimer can be constructed by starting

with an AFM dimer (Atom 1, Atom 2) with release of its coupling to the third atom (Atom 3), as shown in Fig. 4(c). The ground state $|S_A>$ can be further split due to magneto-crystalline effect, giving rise to the first excitation step (the dip) at the small bias voltage. The red-shifting of the second step suggests that the second excited state must be $|S_A+1>$, which requires an overall FM-like coupling between the dimer and the third Mn atom ($J_{12} > 0$, J_{13} and $J_{23} < 0$), as schematically shown in Fig. 4(c). This observation can further exclude the configuration shown in Fig. 3(b) that requires two AFM couplings.

In order to determine spin configuration of the trimer and understand its underlying spin coupling, we have adopted the inelastic tunneling model to evaluate tunneling current [39]:

$$I(V) = \sum_{M,M',\alpha,s=\pm} P_M |\langle M|\mathbf{S}^\alpha|M'\rangle|^2 \frac{eV - s\Delta_{M',M}}{1-e^{-s\beta(eV-s\Delta_{M',M})}} \quad (1)$$

where |M>, |M'> are the initial and final spin states, $\Delta_{M',M}$ is their energy difference, and $\boldsymbol{S}^\alpha = \sum_i \eta_i S_i^\alpha$ is the combined spin operator of the trimer that couples to the tip in the tunneling process. We found that a trimer with symmetric FM spin coupling (Fig. 3(d), $J_{13} \approx J_{23}$) provides the best agreement with our experimental data (see also Fig. S5). Figure 4(a) shows our computed field-dependent spectroscopic curves for a Mn trimer with parameters of J_{12} = 8.9 meV, $J_{13} = J_{23}$ = -1.3 meV and D = -0.08 meV (where D is the magneto-crystalline anisotropy energy. see Supplementary S5.), with assignment of the first three spin excitation steps (from |5/2, -5/2>(n = 0) to |5/2, -3/2>(n = 0), |7/2, -7/2>(n = 1), and |5/2, -3/2>(n = 2)) in Fig. 4(d), where n denotes principal quantum number of electronic state [6, 39]. The transitions indicated by the blue, red and black lines are well consistent with the observed dependence of all three stepwise features on the external magnetic field, as presented in Fig. 4(b). Importantly, the corresponding simulated curves reproduce blueshifts of both the first and third steps, as well as redshifts of the second step at higher fields, and are in good agreement with our experimental data. Therefore, we can safely assign the spin configuration in Fig. 3(d) for our observed trimer.

Our observation and assignment of non-collinear Mn trimer has immediately raised one important question concerning the underlying spin exchange mechanism. In particular, the non-collinear Mn trimer in Fig. 4 has revealed an unusual distance dependent spin coupling between two confined Mn atoms, switching from AFM coupling with short inter-atomic separation (~ 2.7 Å) to FM coupling at a much larger separation (~ 6.3 Å). The measured J_{FM} value of -1.3 meV at the large

separation cannot be simply understood by direct spin exchange interaction between two Mn atoms. We have found that the J_{FM} due to direct spin exchange mechanism with the same range of inter-atomic separation is only about -0.2 meV (Supplementary S4), which is almost six times smaller than our experimental value. This is also consistent with typical rapid decay (i.e. the Bethe-Slater dependence) of direct spin exchange interaction between two localized magnetic moments [47]. It is worth noting while direct spin coupling between two magnetic moments at the unusual long distance has been recently observed due to spatially extended atomically modulated spin texture by atomic scale hydrogen adsorption [48], this mechanism cannot be applied here because of the absence of H atoms and different spatial extension feature in our system (see Supplementary S3). As a result, non-local indirect spin exchange coupling process originating from graphene host needs to be considered. In the graphene/Ru system, strong electronic coupling can lead to high doping concentration of conduction carrier in a single layer graphene through the interfacial electron transfer, which has been experimentally confirmed [27, 28]. These heavily doped conduction carriers in graphene can therefore provide a host coupling to Mn atoms to mediate their spin exchange interactions non-locally through RKKY mechanism, with characteristic decay rate of $\sim 1/d^2$ relationship (where d is the inter-atomic distance). This qualitatively agrees well with our experimental observation of distance dependent decay of J in the non-collinear trimer: $|J_{23}/J_{12}| \sim (d_{23}/d_{12})^{-2}$. We have further evaluated doping carrier concentration in graphene originating from the intrinsic Ru-graphene contact by following established DFT framework [49], and found that the doping carrier concentration can be up to $\sim 1.0 \times 10^{14}$ /cm^2 based on Fermi energy shift [50]. This estimated carrier concentration provides RKKY characteristic switching length scale in range of 7 Å, which is again consistent with our observation of large FM coupling distance in trimer (~ 6.3 Å). All these experimental evidences unanimously support that the graphene/Ru can indeed mediate non-local spin exchange interaction through the RKKY indirect process [51-53]. More control experiments in the future by, for example, comparing trimers confined in different graphene-metal templates with tunable carriers doping, should shed more in-depth insight of relevant mechanism.

In conclusion, we have demonstrated for the first time observation of unique spatial modulation of spin coupling in both Mn dimers and trimers that are regulated by the graphene/Ru substrate. Due to templating effect through moiré superlattice, the Mn nanoclusters are only allowed to occupy certain atomic sites in a periodically rippled graphene, whose spin configurations can be determined

by local spectroscopy measurement. In addition, the graphene/Ru plays a significant role in mediating local and non-local spin exchange interactions, leading to intriguing spin characteristics of different Mn clusters. Our work opens up a few exciting research fronts: First, template method can allow formation of uniform and precise spin coupling on a large scale. For example, dimers are found to preferentially stay at the atop-edge site with larger coupling strength; Second, magnetic nanoclusters regulated by graphene template can possess intriguing spin coupling that might not be easy to achieve otherwise, including spin frustrated system; Importantly, spin coupling in this emerging class of magnetic nanostructures can be finely tailored through their host lattice, representing a new playground to better understand and control nanoscale magnetism. In the future, by combining with atomic manipulation [54-56] or maneuvering deposition at different thermal equilibrium conditions (such as deposition rate and substrate temperature), magnetic clusters resided in different graphene-metal substrates with different and desirable spin coupling might be achievable, which thus provides a unique and efficient test bed for exploring various spin couplings, including subtle Dzyaloshinskii-Moriya interaction [57-61] (see Supplementary S5).

Author Information

Corresponding Authors

*E-mail: hmguo@iphy.ac.cn

Notes

The authors declare no competing financial interest.

Acknowledgements

We thank S. Pantellides, Y.Y Zhang at Vanderbilt University for helpful discussions. Work in China was supported by the National “973” Project of China (grants 2013CBA01600, 2013CB932901), the National Natural Science Foundation of China (grants 61274011, 11574363, 61390501, 51325204), the Chinese Academy of Sciences, and National Supercomputing Center of Tianjin. M.O.

acknowledges supports from the Department of Energy (DESC0010833), National Science Foundation (DMR1608720) and the Office of Naval Research (N000141410328).

References

[1] A. A. Khajetoorians, J. Wiebe, B. Chilian, S. Lounis, S. Blügel, and R. Wiesendanger, Nat. Phys. **8**, 497 (2012).

[2] L. Zhou, J. Wiebe, S. Lounis, E. Vedmedenko, F. Meier, S. Blügel, P. H. Dederichs, and R. Wiesendanger, Nat. Phys. **6**, 187 (2010).

[3] M. Bazarnik, J. Brede, R. Decker, and R. Wiesendanger, ACS Nano **7,** 11341 (2013).

[4] A. Mugarza, N. Lorente, P. Ordejón, C. Krull, S. Stepanow, M.-L. Bocquet, J. Fraxedas, G. Ceballos, and P. Gambardella, Phys. Rev. Lett. **105,** 115702 (2010).

[5] A. J. Heinrich, J. A. Gupta, C. P. Lutz, and D. M. Eigler, Science **306**, 466 (2004).

[6] C. F. Hirjibehedin, C. P. Lutz, and A. J. Heinrich, Science **312**, 1021 (2006).

[7] H. C. Manoharan, C. P. Lutz, and D. M. Eigler, Nature (London) **403**, 512 (2000).

[8] P. Gambardella, A. Dallmeyer, K. Maiti, M. C. Malagoli, W. Eberhardt, K. Kern, and C. Carbone, Nature (London) **416**, 301 (2002).

[9] F. Silly, M. Pivetta, M. Ternes, F. Patthey, J. P. Pelz, and W.-D. Schneider, Phys. Rev. Lett. **92**, 016101 (2004).

[10] S. Loth, S. Baumann, C. P. Lutz, D. M. Eigler, and A. J. Heinrich, Science **335**, 196 (2012).

[11] F. Donati, Q. Dubout, G. Autès, F. Patthey, F. Calleja, P. Gambardella, O. V. Yazyev, and H. Brune, Phys. Rev. Lett. **111**, 236801 (2013).

[12] F. Donati, L. Gragnaniello, A. Cavallin, F. D. Natterer, Q. Dubout, M. Pivetta, F. Patthey, J. Dreiser, C. Piamonteze, S. Rusponi, and H. Brune, Phys. Rev. Lett. **113**, 177201 (2014).

[13] A. H. Castro Neto, N. M. R. Peres, K. S. Novoselov, and A. K. Geim, Rev. Mod. Phys. **81**, 109 (2009).

[14] S. Das Sarma, S. Adam, E. H. Hwang, and E. Rossi, Rev. Mod. Phys. **83**, 407 (2011).

[15] Q. H. Wang, and M. C. Hersam, Nat. Chem. **1,** 206 (2009).

[16] J. M. Macleod, and F. Rosei, Small. **10,** 1038 (2014).

[17] F. Huttmann, A. J. Martínez-Galera, V. Caciuc, N. Atodiresei, S. Schumacher, S. Standop, I. Hamada, T. O. Wehling, S. Blügel, and T. Michely, Phys. Rev. Lett. **115**, 236101 (2015).

[18] G. Berghäuser, and E. Malić, Carbon. **69,** 536 (2014).

[19] J. Ren, H. Guo, J. Pan, Y. Y. Zhang, X. Wu, H. G. Luo, S. Du, S. T. Pantelides, and H. J. Gao, Nano Lett. **14**, 4011 (2014).

[20] A. Bergman, L. Nordström, A. B. Klautau, S. Frota-Pessôa, and O. Eriksson, Phys. Rev. B **73,** 174434 (2006).

[21] S. Lounis, P. Mavropoulos, R. Zeller, P. H. Dederichs, and S. Blügel, Phys. Rev. B **75,** 174436 (2007).

[22] S. Lounis, P. H. Dederichs, and S. Blügel, Phys. Rev. Lett. **101,** 107204 (2008).

[23] S. Holzberger, T. Schuh, S. Blügel, S. Lounis, and W. Wulfhekel, Phys. Rev. Lett. **110,** 157206 (2013).

[24] J. H. Mao, H. G. Zhang, Y. H. Jiang, Y. Pan, M. Gao, W. D. Xiao, and H. J. Gao, J. Am. Chem. Soc. **131**, 14136 (2009).

[25] Y. Pan, M. Gao, L. Huang, F. Liu, and H.-J. Gao, Appl. Phys. Lett. **95**, 093106 (2009)

[26] L.Z. Zhang, S.X. Du, J.T. Sun, L. Huang, L. Meng, W.Y. Xu, L.D. Pan, Y. Pan, Y.L. Wang, W.A. Hofer and H.-J. Gao, Adv. Mater. Interfaces. **1**, 1300104, (2014).

[27] P. Sutter, M. S. Hybertsen, J. T. Sadowski, and E. Sutter, Nano Lett. **9**, 2654 (2009).

[28] M. Gao et al., Appl. Phys. Lett. **96**, 053109 (2010).

[29] Y. Pan, D. X. Shi, and H. J. Gao, Chinese Physics **16**, 3151 (2007).

[30] Y. Pan, H. G. Zhang, D. X. Shi, J. T. Sun, S. X. Du, F. Liu, and H. J. Gao, Adv. Mater. **21**, 2777 (2009).

[31] P. Wahl, P. Simon, L. Diekhoner, V. S. Stepanyuk, P. Bruno, M. A. Schneider, and K. Kern, Phys. Rev. Lett. **98**, 056601 (2007).

[32] O. O. Brovko, P. A. Ignatiev, V. S. Stepanyuk, and P. Bruno, Phys. Rev. Lett. **101**, 036809 (2008).

[33] N. Néel, R. Berndt, J. Kröger, T. O. Wehling, A. I. Lichtenstein, and M. I. Katsnelson, Phys. Rev. Lett. **107**, 106804 (2011).

[34] J. Ren, X. Wu, H. Guo, J. Pan, S. Du, H.-G.Luo, and H.-J. Gao, Appl. Phys. Lett. **107**, 071604 (2015).

[35] T. Sachse, N. Néel, S. Meierott, R. Berndt, W. A. Hofer, and J. Kröger, New J. Phys. **16,** 063021 (2014).

[36] See Supplemental Material [url] for identifying Mn dimers and trimers, which includes Refs. [37, 38].

[37] P. Bevington and D.K. Robinson, Data Reduction and Error Analysis for the Physical Sciences

(McGraw-Hill 2002)

[38] L. Liu, K. Yang, Y. Jiang, B. Song, W. Xiao, L. Li, H. Zhou, Y. Wang, S. Du, M. Ouyang, W.□A. Hofer, A.□H. Castro Neto, and H.-J. Gao, Sci. Rep. **3**, 1210 (2013).

[39] J. Fernández-Rossier, Phys. Rev. Lett. **102,** 256802 (2009).

[40] See Supplemental Material [url] for DFT method, which includes Refs. [41-46].

[41] G. Kresse and J. Furthmüller, Phys. Rev. B **54,** 11169 (1996).

[42] G. Kresse and J. Furthmüller, Comp. Mater. Sci. **6,** 15 (1996).

[43] P. E. Blöchl, Phys. Rev. B **50,** 17953 (1994).

[44] G. Kresse and D. Joubert, Phys. Rev. B **59,** 1758 (1999).

[45] S.□L. Dudarev, G.□A. Botton, S.□Y. Savrasov, C.□J. Humphreys, and A.□P. Sutton, Phys. Rev. B 57, 1505 (1998).

[46] L. Wang, T. Maxisch, and G. Ceder, Phys. Rev. B 73, 195107 (2006).

[47] J. Stöhr and H. C. Siegmann, Magnetism: From Fundamentals to Nanoscale Dynamics (Springer-Verlag, Berlin, 2006).

[48] H. Gonzalez-Herrero, J. M. Gomez-Rodriguez, P. Mallet, M. Moaied, J. J. Palacios, C. Salgado, M. M. Ugeda, J.-Y. Veuillen, F. Yndurain, and I. Brihuega, Science **352,** 437 (2016).

[49] G. Giovannetti, P. A. Khomyakov, G. Brocks, V. M. Karpan, J. van den Brink, and P. J. Kelly, Phys. Rev. Lett. **101**, 026803 (2008).

[50] H. G. Zhang, J. T. Sun, T. Low, L. Z. Zhang, Y. Pan, Q. Liu, J. H. Mao, H. T. Zhou, H. M. Guo, S. X. Du, F. Guinea, and H.-J. Gao, Phys. Rev. B **84**, 245436 (2011).

[51] See Supplemental Material [url] for Analysis of RKKY interaction of Mn adatoms on graphene layers, which includes Refs. [52-53].

[52] C. Berger et al., Science **312**, 1191 (2006).

[53] H. Zhang et al., Phys. Rev. Lett. **110**, 066805 (2013).

[54] D. M. Eigler and E. K. Schweizer, Nature (London) **344**, 524 (1990).

[55] D. M. Eigler, C. P. Lutz, and W. E. Rudge, Nature (London) **352**, 600 (1991).

[56] J. A. Stroscio and D. M. Eigler, Science **254**, 319 (1991).

[57] V. E. Dmitrienko, E. N. Ovchinnikova, S. P. Collins, G. Nisbet, G. Beutier, Y. O. Kvashnin, V. V. Mazurenko, A. I. Lichtenstein, and M. I. Katsnelson, Nat. Phys. **10**, 202 (2015).

[58] See Supplemental Material [url] for Analysis of DM interaction, which includes Refs. [59-61].

[59] I. Dzyaloshinsky, J. Phys. Chem. Solids **4**, 241 (1958)

[60] R. Yanes et al, Phys.Rev.Lett. **111**, 217202 (2013)

[61] A. A. Khajetoorians et al, Nat. Commun. **10**, 202 (2014)

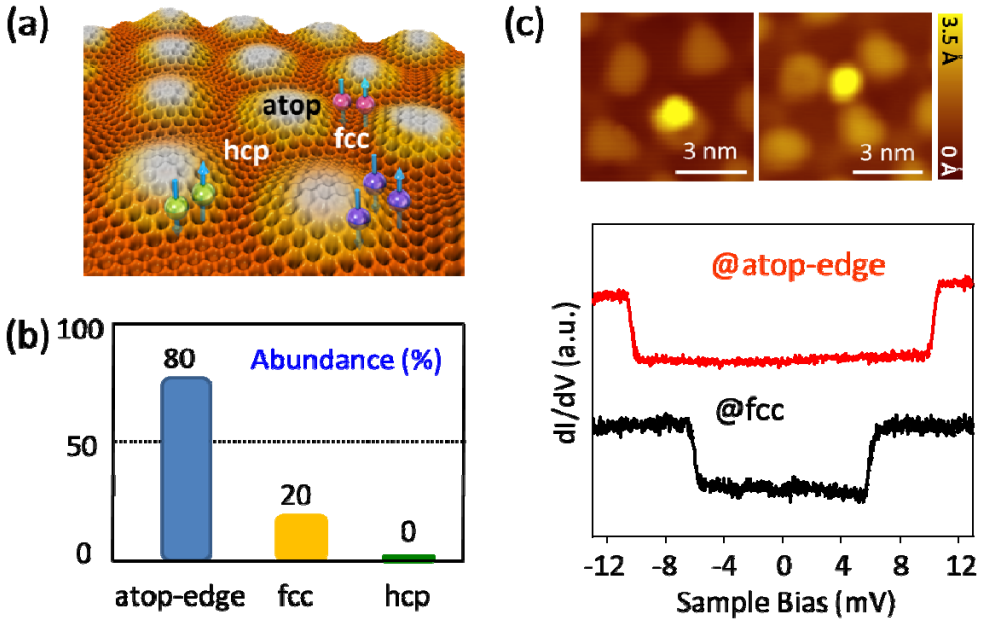

FIG. 1: (a) Schematic view of Mn atomic clusters adsorbed at different regions with respect to the moiré pattern of graphene/Ru(0001); (b) Statistical distribution of ~ 100 Mn dimers adsorbed at different locations. (c) STM images and conductance spectra of Mn dimers adsorbed at different sites, i.e. @atop-edge and @fcc regions of graphene/Ru(0001) surface.

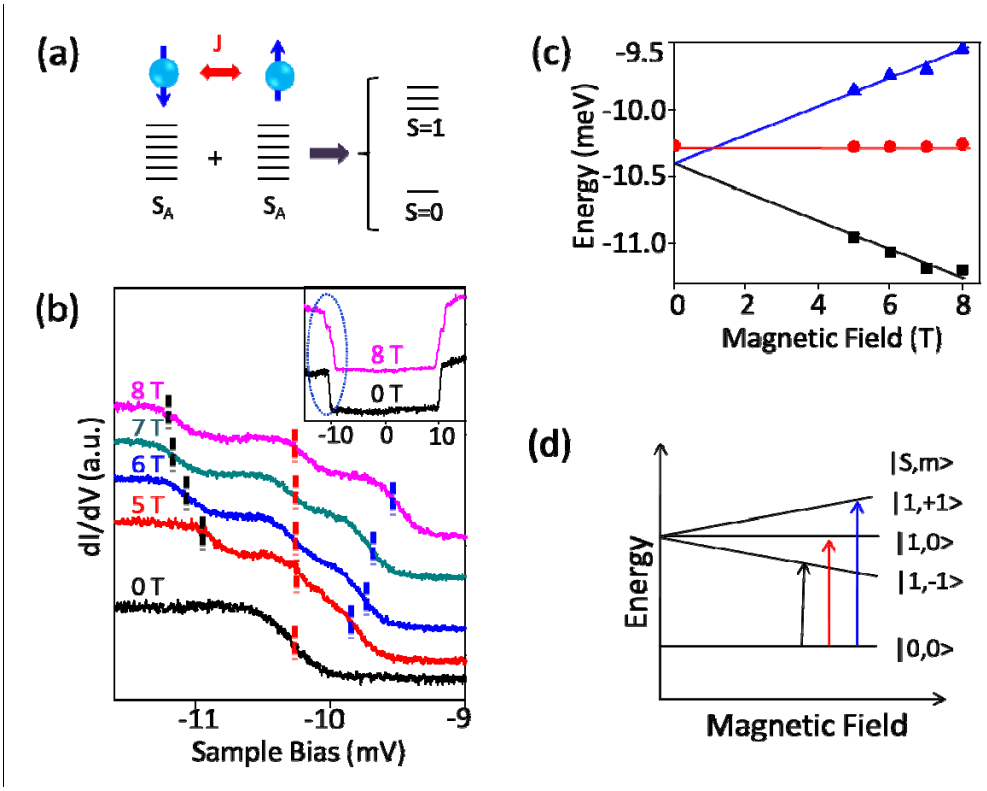

FIG. 2: (a) AFM coupling of Mn dimer with $2S + 1$ degeneracy for the S multiplets. (b) Spectroscopic measurements taken on Mn dimer at B = 0, 5, 6, 7 and 8 T, respectively. Each curve is vertically shifted for clarity. Inset shows the same spectra over a larger energy range for B field of 0 T and 8 T. (c) Summary of magnetic field dependence of step energies acquired from the IETS spectra for low (black squares), medium (red circles), and high (blue triangles) energy steps in (b). Solid lines are linear fits with $E = E_{\Delta m} + \Delta m g \mu_B B$. (d) Schematic of the tunneling induced transitions between singlet (|0, 0>) and triplet (|1, -1>, |1, 0> and |1, +1>) states at the presence of magnetic field. S and m are the total spin value and the magnetic quantum number, respectively.

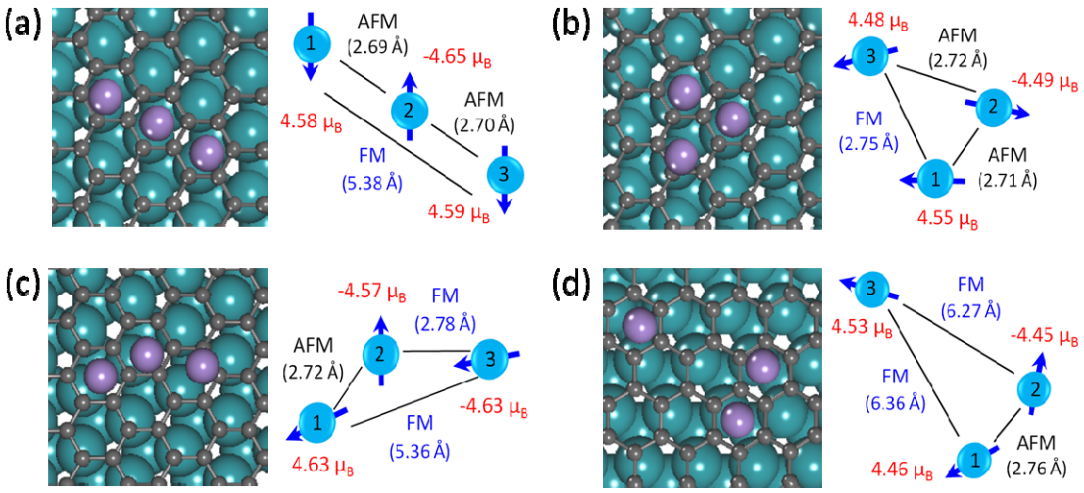

FIG. 3: Four optimized stable configurations of Mn trimers adsorbed at the atop-edge region on the graphene/Ru(0001) substrate obtained from the DFT calculations (left), and the sketch diagram of their corresponding magnetic coupling (right). The optimized Mn configurations can be classified into two categories according to their inter-atomic spin couplings: AFM-AFM-FM ((a) and (b)) and AFM-FM-FM ((c) and (d)).

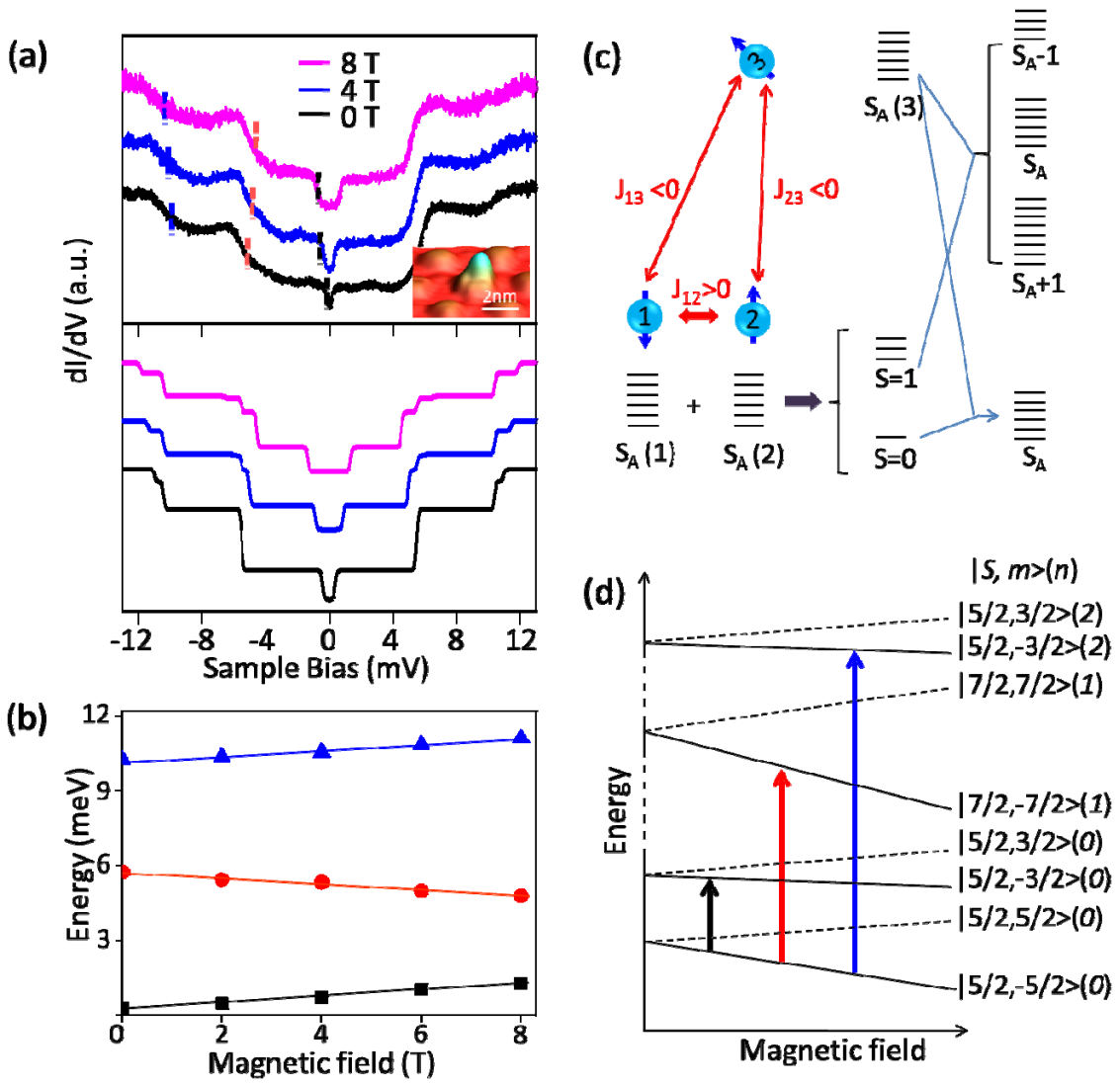

FIG. 4: (a) (Top) The field-dependent conductance spectra performed on a Mn trimer show several symmetric stepwise features around the Fermi level. Inset shows STM topography of the Mn trimer on graphene/Ru(0001) for measurement. (Bottom) Theoretical field dependent conductance spectra of Mn trimer by using an AFM-FM-FM model (J_{12} = 8.9 meV, J_{13} = J_{23} = -1.3 meV and D = -0.08 meV for computation). (b) Magnetic field dependence of step energies from the IETS spectra in (a). (c) Schematic energy diagram of a Mn trimer involving two atoms with antiferromagnetic interaction and the third one with ferromagnetic coupling to the other two atoms. (d) Illustration of the tunneling induced spin states transitions at the presence of magnetic field. The allowed transitions meet selection rule of $\Delta m = \pm 1$, which are highlighted by vertical arrows. The n represents principal quantum number. The (n = 0, 1, 2) indicate the ground state, the first and second excited states, respectively.